Structural Colors in Nature

and Butterfly-Wing Modeling

Gérard Tayeb, Boris Gralak
and Stefan Enoch

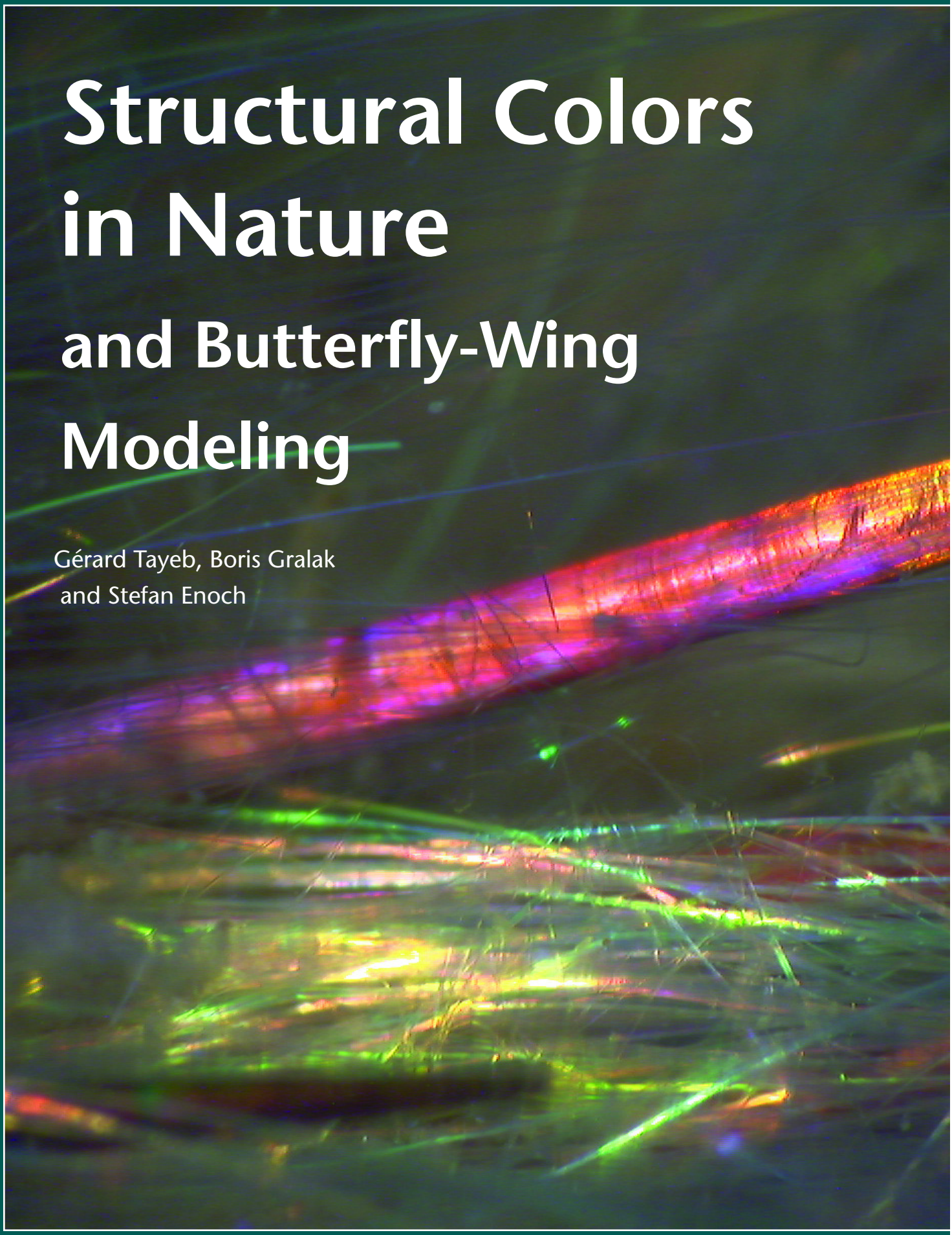

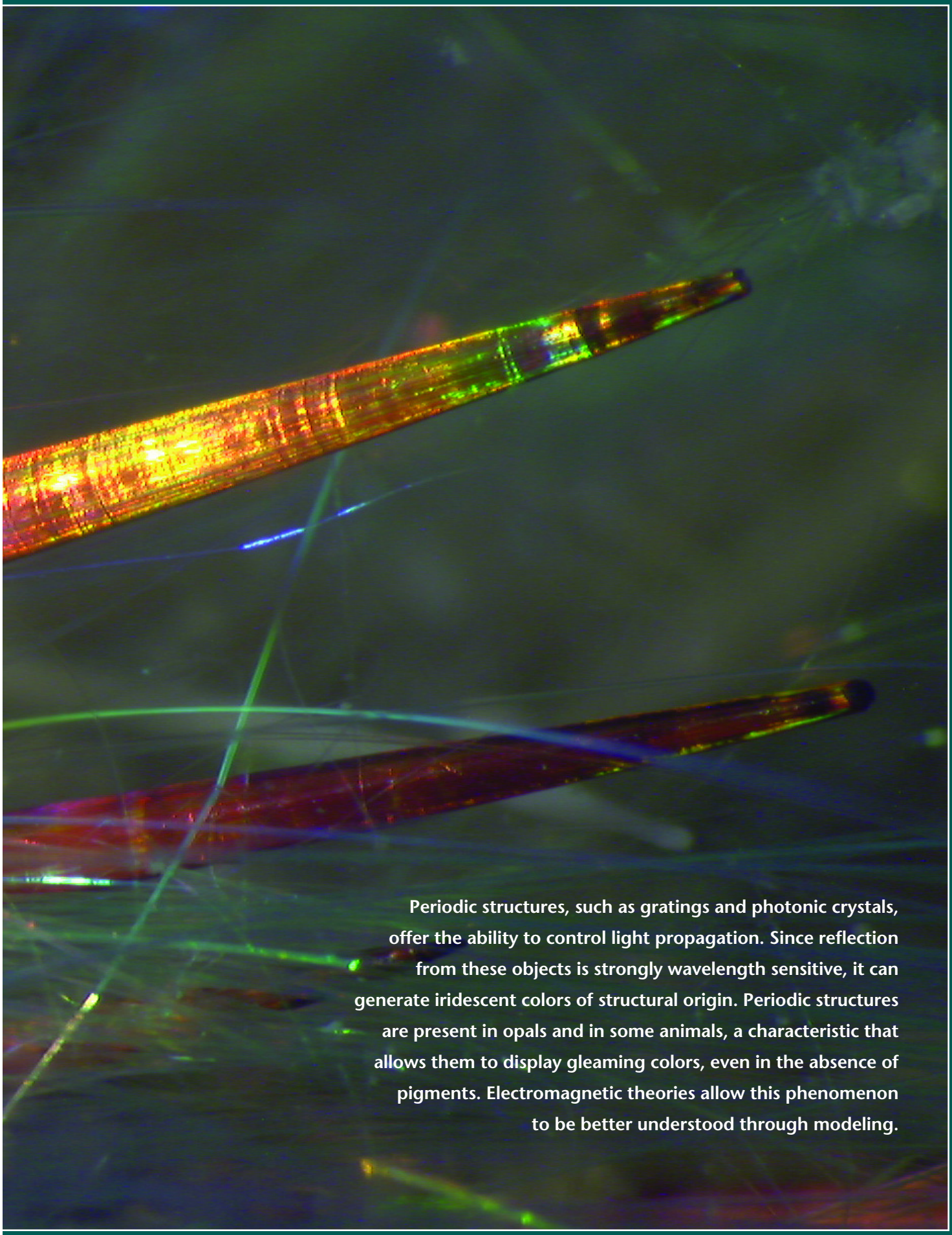

Periodic structures, such as gratings and photonic crystals, offer the ability to control light propagation. Since reflection from these objects is strongly wavelength sensitive, it can generate iridescent colors of structural origin. Periodic structures are present in opals and in some animals, a characteristic that allows them to display gleaming colors, even in the absence of pigments. Electromagnetic theories allow this phenomenon to be better understood through modeling.

Iridescent threads and spines of a sea mouse. [From http://www.physics.usyd.edu.au/~nicolae/seamouse.html]

Over the course of recent years, numerous research groups have devoted increasing attention to photonic band structures. These structures, which are composed of a periodic arrangement of dielectric materials, are unique in that, although they are made of transparent materials, they can inhibit the propagation of light over some wavelength ranges. The range of wavelengths over which the passage of light is inhibited is known as a bandgap. Photonic band structures soon may find commercial application in devices that entail the inhibition of spontaneous emission, such as laser diodes and high-efficiency light-emitting diodes, as well as in integrated optics components, such as waveguides and wavelength multiplexers for optical telecommunications.

The structural control of light is manifest in the animal and mineral worlds, as well as in the realm of high technology. The oldest and best-known example is the opal, a sedimentary gem used as far back as the early Aztecs. Unlike other mineral gems, the opal does not have a crystalline structure. It is made of tiny spheres of silica packed together. The diffraction of light through this arrangement produces a characteristic play of colors, the nature of which is determined by the size of the spheres and the regularity of the periodic structure. Researchers have drawn inspiration from these gems to build artificial opals by sedimentation of spheres. This is one of the two principal techniques used for building three-dimensional (3D) photonic crystals.

At the University of Sydney, Australia, a research group headed by Professor Ross C. McPhedran has discovered that photonic crystals are also present in the animal world,[1] specifically in the sea mouse, a marine worm found in moderately deep water. The sea mouse is partly covered with long, feltlike threads that produce a brilliant iridescence, a range of colors that changes with the direction of the incident light and the direction of observation. It is also characterized by iridescent spines. Both threads and spines are clearly visible in the photograph on the preceding pages. A scanning electron microscope (SEM) image of a cross-section of a thread or of a spine reveals a periodic microstructured pattern with hexagonal symmetry. Numerical studies have shown that these 2D photonic crystals possess a partial bandgap (i.e., for some directions of propagation of light), which is the physical explanation of their iridescence.

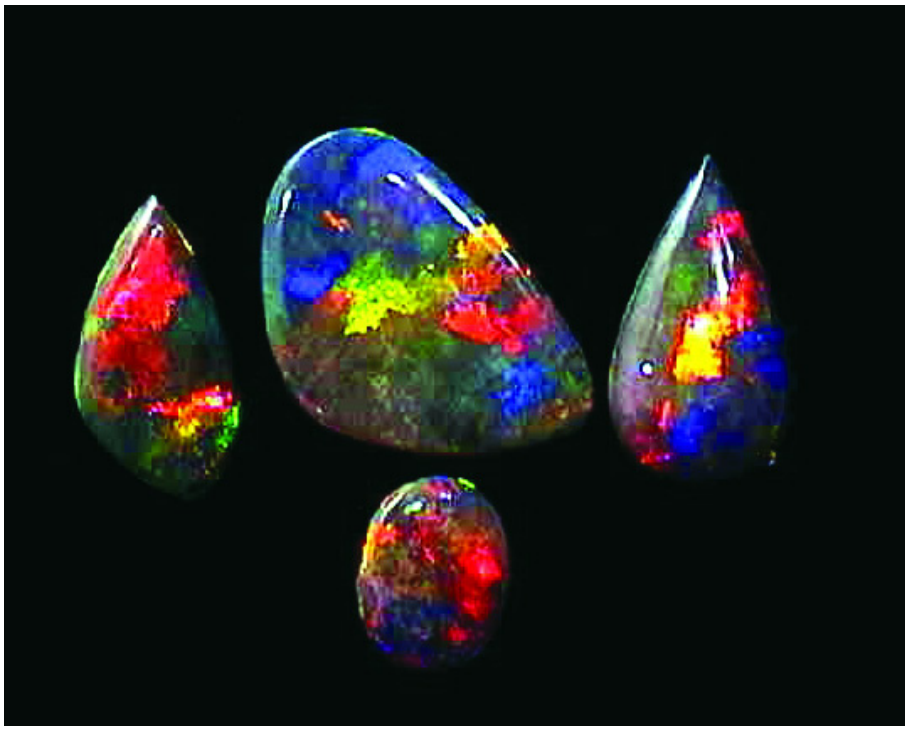

Figure 1. The opal is perhaps the best-known example of photonic band structures in nature. [From http://www.roughcutgems.com/]

It is worth noting that, in the case of the opal and the sea mouse, the colors are generated by the structural properties of the objects themselves. They are caused, in other words, by interference, or more specifically by the light-diffracting characteristics of the microstructure, not by selective absorption or reflection of light by pigments, the most common origin of colors.

Let us now consider the butterfly, a species in which color is generally produced in both of the ways described above. In butterflies, color plays an important role in thermal regulation, communication and camouflage. For some butterflies, such as the *Morpho rhetenor*, one way of producing color predominates. The iridescent blue color of the *Morpho rhetenor*, an extremely metallic and iridescent butterfly that lives in South America, comes from diffraction by the microstructure of its wings. Blue pigments are, in fact, very uncommon in nature. The wingspan of *Morpho rhetenor* is about 12 cm. Its wings consist of a membrane covered with layers of scales. The bottom layer is composed of structural scales that produce color, while the upper layer does not contribute to the production of color.[2] The scales, each of which is about 200 μm long and 80 μm wide, are made of chitin and covered with about 1300 thin, parallel ridges per millimeter. This periodic structure constitutes a diffraction grating, the cross-section of which exhibits a tree-like geometry.

In keeping with grating theory, the study of the microstructure, because of its very fine scale, requires that the vectorial nature of light (polarization) be taken into account. The numerical methods developed to solve Maxwell's equations can be used to study this complex problem.[3] Here we model the scale as a multilayered grating of ribs, as shown in Fig. 4. The figure shows field maps for two wavelengths corresponding to the colors blue and red. The scale is illuminated from the top in normal incidence and in E// polarization (the electric field

1047-6938/03/02/0038/6-$0015.00

is perpendicular to the figure). It is evident that blue is strongly reflected (the field on the field map below the structure is weak) while red is not. For $\lambda = 0.6\ \mu m$, we observe that the field propagates inside the structure along the dielectric regions. The scale structure in the region between the ridges and the bottom membrane is actually rather complex and disordered, with probable inclusion of pigments. This means that the longer wavelengths that pass through the tree-like grating are much more sensitive to the bottom region of the scale. If the absorption phenomenon in the actual scale were mainly caused by localized effects inside the pigments (or other absorbing defaults), it would explain the absorption of red light observed in the experiments.[4]

Strong chromatic selection is also evident in the reflection curves for both E// and H// polarizations (electric and magnetic field perpendicular to the figure, respectively). Indeed, the structure of the butterfly wing works as a short-wave-pass filter for the reflected waves. For this reason, one can infer that the color produced will be blue.

Yet colors are, by nature, complex. Although each of us may perceive colors slightly differently, both the eye and the brain always play important roles in color perception. Standard conditions for performing color measurement experiments have been formulated by the Commission Internationale de l'Éclairage (CIE). By use of reference stimuli, the CIE has defined a standard set of tristimulus values to match each wavelength of the spectrum.

Let us now summarize the basic ideas for converting reflection coefficients into color maps. We assume that the body under study is illuminated by an illuminant characterized by its energy distribution $D(\lambda)$. In this article, we use the CIE normalized illuminant D65, which closely matches that of the sky in conditions of daylight.[5,6]

Assuming that the body has a reflectivity $R(\lambda)$, we can compute the CIE XYZ tristimulus values,[7] which are one possible way to characterize the reflected color, according to:

$$X = \frac{1}{k}\int D(\lambda)\ R(\lambda)\ \bar{x}(\lambda)\,d\lambda$$

$$Y = \frac{1}{k}\int D(\lambda)\ R(\lambda)\ \bar{y}(\lambda)\,d\lambda$$

$$Z = \frac{1}{k}\int D(\lambda)\ R(\lambda)\ \bar{z}(\lambda)\,d\lambda$$

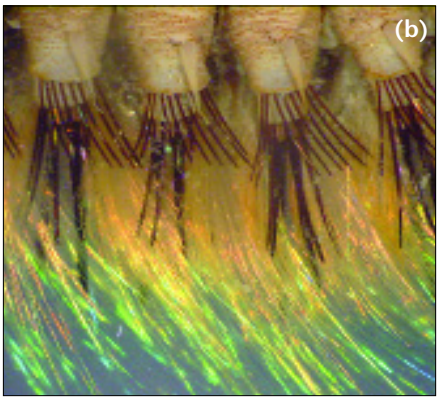

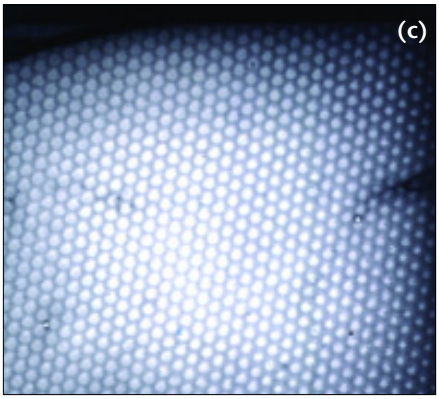

Figure 2. (a) Sea mouse, (b) its iridescent threads, (c) SEM cross-section of a spine. [From http://www.physics.usyd.edu.au/~nicolae/seamouse.html].

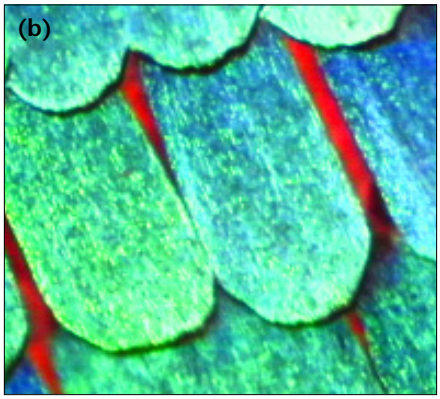

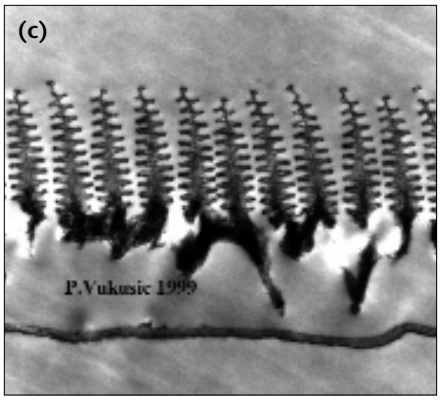

Figure 3. *Morpho rhetenor* butterfly. (a) A drop of alcohol modifies the index contrast and consequently changes the color from blue to green. (b) Detail of the scales. (c) Transmission electron microscope image showing cross-section of a scale. [*Courtesy Pete Vukusic, Exeter University*].

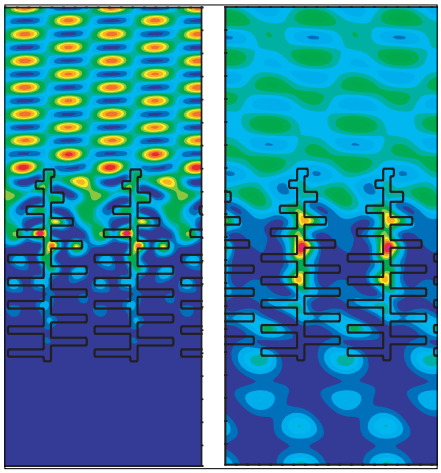

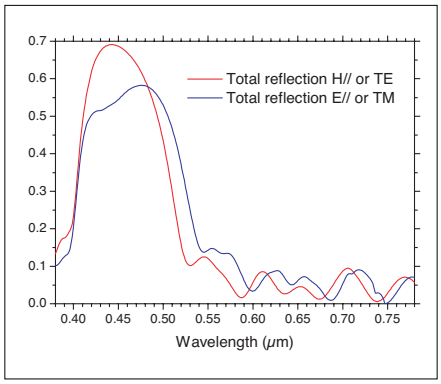

Figure 4. Field map of the electric field modulus for λ = 0.42 μm (left, blue) and λ = 0.60 μm (right , red). The color map goes from blue (no field) to red (maximum value of the field). The curve gives the total reflection and transmission for both polarizations. [From Ref. 3].

Here, the weighting functions $\bar{x}, \bar{y}, \bar{z}$ (Fig. 5) are the CIE 1964 spectral tristimulus values[6,8] and k is a normalization factor defined in such a way that an object with a uniform reflectivity $R(\lambda) = 1$ gives a luminance component Y equal to 1:

$$k = \int D(\lambda)\, \bar{y}(\lambda)\, d\lambda$$

Because of the spectral bandwidth of the human eye, the only values of the wavelength that we will retain lie in the 0.38-0.78 μm range.

We then transform the XYZ components into RGB components, which are more convenient for the imaging process. Since RGB values are device dependent, we use the International Telecommunication Union recommendation BT.709, which is representative of contemporary monitors in studio video, computing and computer graphics. In this case, the conversion is given by the linear transformation[7]:

$$\begin{bmatrix} R \\ G \\ B \end{bmatrix} = \begin{bmatrix} 3.240479 & -1.537150 & -0.498535 \\ -0.969256 & 1.875992 & 0.041556 \\ 0.055648 & -0.204043 & 1.057311 \end{bmatrix} \begin{bmatrix} X \\ Y \\ Z \end{bmatrix}$$

These RGB values are normalized and should remain between 0 and 1. In fact, they can in some cases be slightly less than 0 or greater than 1. This means that the color cannot be accurately represented on such monitor devices by additive reproduction of these RGB values. In this case, the values are rounded to 0 or 1.

The final step in the process is color representation. For this purpose, one can use the Portable PixMap (PPM) file format, a text file in which one simply enters the RGB values for each pixel. Note that each RGB value should be an integer between 0 and 255, obtained by scaling the values obtained from the linear transformation above. These PPM files can be easily displayed on a computer screen using classical image editors. It is also easy to print the files.

At this stage, we have replaced a complicated set of data [i.e., the spectrum $R(\lambda)$] by a color point in a color map. As illustrated below, this type of representation can be used to obtain an overall per-

spective of the reflection properties of a body. A 2D color map based on this representation provides two free parameters (for example, the two angles of diffraction).

Let us now suppose that the butterfly wing is illuminated by skylight, and that we want to determine the color reflected by the wing in a direction characterized by the polar angle θ (the angle between the normal to the wing and the direction of observation) and the azimutal angle φ. To simulate the uniform luminance of the skylight, the incident field is modeled by the superposition of a great number of plane waves illuminating the wing with various incidences coming from the upper half space. To sample the visible spectrum, the calculations are made for several values of the wavelength λ. To obtain the reflectivity $R(\theta,\varphi,\lambda)$ that describes the color spectrum reflected in the (θ,φ) direction, we incoherently add the intensities reflected by the grating. By use of the procedure described above, we transform this function into a RGB(θ,φ)color map.

Figure 6 shows such maps for the structure of Fig. 4. On these maps, the horizontal axis gives the θ value, from 0° to 80°, and the vertical axis gives the φ value, from 0° to 180°. This means that the left side of the maps shows the reflected color in the direction normal to the scale (θ = 0) and the right side gives the reflected color for near grazing angles. The left-hand figure corresponds to the scale while the wing is suspended in the air, while the right-hand one corresponds to the scale while the wing is lying in isopropyl alcohol (IPA), with an optical index of 1.38. Because of the change of index contrast between the scale (the optical index of chitin is close to 1.56) and the embedding media (air or IPA), the diffraction phenomenon is strongly modified by immersion in IPA (the optical paths are roughly changed), and the reflected colors are completely modified. This modeling agrees with the experiment shown in Fig. 3. After evaporation of the IPA, the wing recovers its original blue color, thus confirming the fact that the colors are structural.

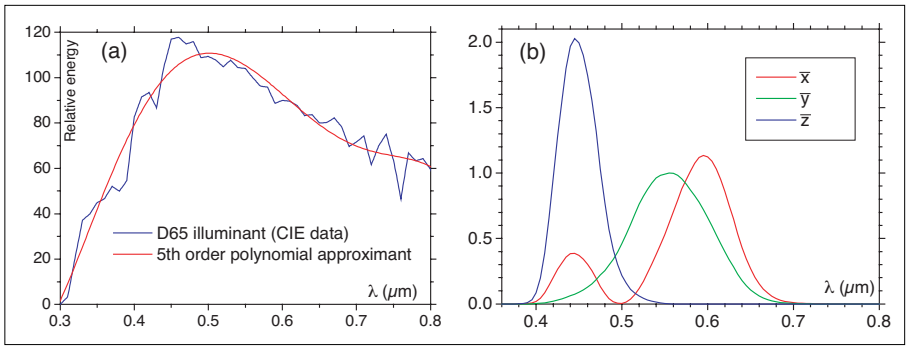

Figure 5. *Left*: Relative energy distribution of D65 illuminant (blue) and its 5th order polynomial approximation used in computations (red) versus wavelength λ. *Right*: Spectral x̄, ȳ, z̄ tristimulus values. [From Ref. 3].

Conclusion

Natural opal gems can serve as a source of inspiration to physicists in the creation of 3D photonic crystals. In butterflies, both structural and chemical processes (pigments) serve to produce colors. In the future, the combination of these two processes of color creation could be used in the realization of textiles for clothing. Indeed, researchers are now studying the incorporation of structural colors in thread. The field of potential applications of the understanding of these processes includes all the domains in which color plays an important role. Automobile manufacturers, for example, sometimes combine pigments and structural properties to produce specific shades of color. In the future, experiments in a number of technological and productive realms will be furthered by the opportunities to create color that are inspired by the opal, the sea mouse, the butterfly wing and other manifestations of color in nature.

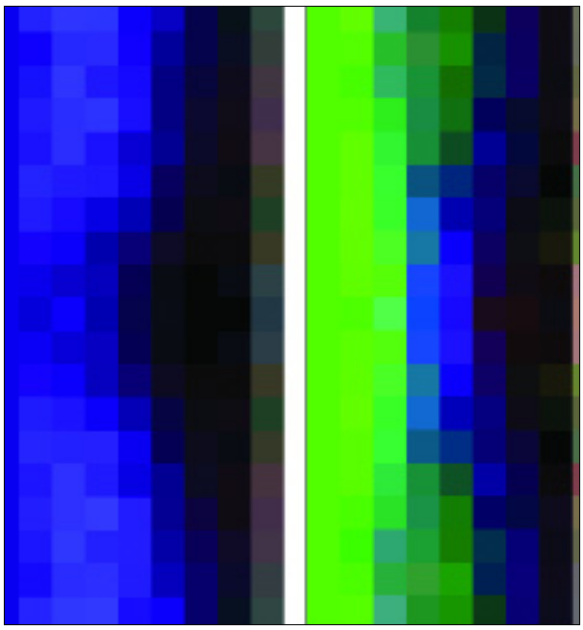

Figure 6. Colors reflected by a butterfly wing scale modeled as in Fig. 4. The horizontal axis gives the θ value, from 0° to 80°, and the vertical axis gives the φ value, from 0° to 180°. The angular shift between two neighboring squares is equal to 10°. The left-hand map corresponds to a scale of the wing suspended in air, while the right-hand one corresponds to a scale of the wing lying in IPA. [From Ref. 3.]

References

Please see OPN Feature Article References, page 49.

Gérard Tayeb, a professor at the Université Aix-Marseille, and Stefan Enoch (stefan.enoch@fresnel.fr), a researcher with the Centre National de la Recherche Scientifique, are both affiliated with the Fresnel Institute, Marseille, France. Boris Gralak occupies a post-doctoral position at FOM-Institute for Atomic and Molecular Physics, Amsterdam, The Netherlands.

Feature Article References

Note: References in OPN feature articles are published exactly as submitted by the authors.

Optoelectronic Microsystems Integration for System-on-a-Package and System-on-a-Chip Applications 26

Nan Marie Jokerst, Martin A. Brooke, Sang-Yeon Cho, Dae-Ik Kim, Mikkel Thomas and Suzanne Fike

1. S. K. Tewksbury and L. A. Hornak, "Optical clock distribution in electronic systems," Journ. VLSI Sig. Pro., vol. 16, 1997, pp. 225-246.
2. Rassaian, M.; Beranek, M.W., "Quantitative characterization of 96.5Sn3.5Ag and 80Au20Sn optical fiber solder bond joints on silicon micro-optical bench substrates," IEEE Trans. on Adv. Pack., vol. 22, 1999, pp. 86-93.
3. S. J. Walker and J. Jahns, "Optical clock distribution using integrated free-space optics," Opt. Comm., vol. 90, 1992, pp. 359-371.
4. P. J. Delfyett, D. H. Hartman, and S. Z. Ahmad, "Optical clock distribution using a mode-locked semiconductor laser-diode system," Journ. of Light. Tech., vol. 9, 1991, pp. 1646-1649.
5. B. Bihari, J. Gan, L, Wu, Y. Liu, S. Tang, and R. T. Chen, "Optical clock distribution in supercomputers using polyimide-based waveguides," Proc., Opto. Intercon. VI., San Jose, CA, Jan. 1999, pp. 123-133.
6. David A. B. Miller, "Rationale and Challenges for Optical Interconnects to Electronic Chips," Proc. of the IEEE, vol. 88, 2000, pp. 728-749.
7. Y. Liu, E. Strezelecka, J. Nohava, M. Hibbs-Brenner, E. Towe, "Smart-Pixel Array Technology for Free-Space Optical Interconnects," Proceedings of the IEEE, vol. 88, No. 6, p. 764-768June, 2000.
8. Jokerst, N.M.; Brooke, M.A.; Laskar, J.; Wills, D.S.; Brown, A.S.; Vrazel, M.; Jung, S.; Joo, Y.; Chang, J.J., "Microsystem optoelectronic integration for mixed multisignal systems," IEEE Journal on Special Topics in Quantum Electronics Millenium Issue, Vol. 6, No. 6, pp. 1231-1239, November/December, 2000.
9. Chang, J.J.; Jung, S.; Vrazel, M.; Jung, K.; Lee, M.; Brooke, M.A.; Jokerst, N., "Hybrid optically interconnected microprocessor: an InP I-MSM integrated onto a mixed-signal CMOS analog/microprocessor IC," Proceedings of the International Society for Optical Engineering, Vol. 4089, pp.708-714, 2000.
10. S. Cho, N. Jokerst, "Polymer waveguide optical interconnections for electrical interconnection substrates," Proceedings of the IEEE Conference on Lasers and Electro-Optics, pp. 161-162, Long Beach, CA, May, 2002.
11. S. Fike, B. Buchanan, N. M. Jokerst, M. Brooke, T. Morris, S. DeWeerth, "8 X 8 Array of Thin Film Photodetectors Vertically Electrically Interconnected to Silicon Circuitry," IEEE Photonics Technology Letters, Vol. 7, No. 10, pp. 1168-1170, October, 1995.
12. S. Wilkinson, J. Tabler, N. Jokerst, M. Brooke, R. Leavitt, "An 8*8 array of resonant cavity enhanced light emitting diodes integrated onto silicon grayscale (32 level) driver circuitry," Proceedings of the IEEE LEOS 9th Annual Meeting, Boston, MA, Vol. 2, p.277-8, Nov. 18-19, 1996.

Femtosecond-Laser-Assisted Microstructuring of Silicon Surfaces for New Optoelectronics Applications 32

James E. Carey, Catherine H. Crouch and Eric Mazur

1. T.-H. Her, R. J. Finlay, C. Wu, and E. Mazur, Appl. Phys. A **70**, 383 (2000).
2. C. Wu, C. H. Crouch, L. Zhao, J. E. Carey, R. Younkin, J. A. Levinson, E. Mazur, R.M. Farrell, P. Gothoskar, and A. Karger, Appl. Phys. Lett. **78**, 1850 (2001).
3. J.-M. Bonard, H. Kand, T. Stockli, and L.-O. Nilsson Solid State Electronics, vol. **45**, p. 893, (2001).
4. A. Pokhmurska, O. Bonchik, S. Kiyak, G. Savitski, A. Gloskovsky, Appl. Surf. Sci. **154-155**, 712-715 (2000).
5. Y. Hatanaka, M. Niraula, A. Nakamura, T. Aoki, Appl. Surf. Sci. **175-176**, 462-467 (2001).
6. E. Janzen, R. Stedman, G. Grossman, and H.G. Grimmeiss, Phys. Rev. B **29**, 1907-1918 (1984).
7. C. Wu, C.H. Crouch, L. Zhao, and E. Mazur, Appl. Phys. Lett. **81**, 1999-2001 (2002).
8. M. Shen, C. H. Crouch, J. E. Carey. R. Younkin, M. Sheehy. C. M. Friend, E. Mazur, submitted to Appl. Phys. Lett.

Structural Colors in Nature and Butterfly-Wing Modeling 38

Gérard Tayeb, Boris Gralak and Stefan Enoch

1. A. R. Parker, R. C. McPhedran, D. R. McKenzie, L. C. Botten and N. A. Nicorovici, "Photonic engineering: Aphrodite's iridescence," Nature 409, 36-37 (2001).
2. H. Ghiradella, "Light and color on the wing: structural colors in butterflies and moths," Applied Optics **30**, 3492-3500 (1991).
3. B. Gralak, G. Tayeb and S. Enoch. "Morpho butterflies wings color modeled with lamellar grating theory," Optics Express Vol. 9, No. 11, 567-578 (2001).
4. P. Vukusic, J.R. Sambles, C.R. Lawrence and R.J. Wootton, "Quantified interference and diffraction in single *Morpho* butterfly scales," Proceedings: Biological Sciences, The Royal Society of London **266**, 1403 -1411 (1999).
5. Colourware, Colour FAQ, http://www.colourware.co.uk/cpfaq.htm
6. CVRL Color & Vision database, http://www.cvrl.org/
7. Charles A. Poynton, Color technology, http://www.poynton.com/ColorFAQ.html
8. Color Science, http://www.physics.sfasu.edu/astro/color.htm